

# FLOWS AND BEDLOAD DYNAMICS AROUND SPUR DYKE IN A COMPOUND CHANNEL

Y Baba<sup>1</sup>, B Camenen<sup>2</sup>, Y Peltier<sup>2</sup>, F Thollet<sup>2</sup> and H. Zhang<sup>1</sup>

1. Ujigawa Hydraulics Laboratory, DPRI, Kyoto University, Yoko-Oji, Fushimi, Kyoto, 612-8235, Japan
2. Cemagref, UR HHLY, 3 bis quai Chauveau, CP 220, 69336 Lyon cedex 09, France

## ABSTRACT

Spur dykes are typical man-made hydraulic structures and widely used in alluvial rivers for a variety of purposes like the bank protection, the maintenance of navigation channel and so on. Spur dykes give some impacts on the flow and bedload dynamics around itself and cause the variation of flow pattern and bottom profile according to the relationship between the flow characteristics and bed configurations. In the case of a compound channel with a spur dyke on the floodplain, the effect of the spur dyke on the flow and bed configuration makes the flow characteristics complicated. In order to investigate the flow characteristics around the spur dyke, some experimental studies have been carried out using the LSPIV technique and an electromagnetic velocimeter. The velocity distributions around spur dykes are discussed in combination with the type of the spur dykes and the relative depth  $H_r$  (the ratio of the water depth in the floodplain and main channel). The longitudinal length of the recirculation area is discussed as well. The difference of the flow pattern around the foot of the spur dyke between impermeable and permeable cases also illustrated based on the experimental results, and it is found that the permeable spur dyke appears to be a much more interesting alternative to the impermeable spur dyke in term of morphodynamics around the spur dyke.

## 1 INTRODUCTION

Spur dykes are typical man-made hydraulic structures and widely used in alluvial rivers to expect some positive effects for disaster reduction and river restoration. Spur dykes are classified in two types according to its structure, impermeable and permeable types. The existence of the spur dykes brings significant changes of flow patterns and bed configurations around the spur dykes (Zhang et al., 2009). The change of the flow pattern initiates and controls the bottom profile variation, and the flow pattern adjusts itself according to the bed configurations. The interaction of these processes (flow and bottom profile) develops the river morphology and leads to an equilibrium stage of flow and bed configurations under certain conditions. Local scour is well-known to be generated around the spur dykes, and it is the result of the combined processes with flow and movable boundaries. It is also well known that an excessive scouring sometimes occurs and causes enormous damage.

This study discusses compound channel flows occurring in a vicinity of a non-submerged spur dyke set on the floodplain. In the case of a compound channel, the interaction between the flow and the bottom profile would be more complicated because the influence of the spur dykes causes the enhancement of the momentum transfer and the mass exchange between the floodplain and the main channel (Peltier et al., 2008). This means that quantitative information of flow pattern around the spur dykes is strongly required in order to investigate the interaction between the flow characteristics and bed configurations.

In this paper, some experimental results on the velocity distributions around the spur dykes are shown, and the effects of the spur dykes (impermeable and permeable) on the flow characteristics is discussed. Additionally some likely impacts of the flow characteristics on the bed configurations, especially bedload transportation, are also discussed based on the experimental results.

## 2 PRESENTATION OF THE EXPERIMENT AND MEASUREMENTS

### 2.1 Flume characteristics and experimental set-up

An experimental study was set up in a 20m long straight compound channel (Ujigawa laboratory, Kyoto, Japan). The slope was set to 0.8/1000. The total width of the channel is 1m with a main channel width of 0.35m (see Figure 1). A single floodplain was set on the right part of the channel with a step of 5.1cm. Two types of spur dyke set on the floodplain were explored, one is impermeable and the other is permeable (set of piers inducing a permeability of 50%). The effects on the flow of the length of the spur dyke were studied as well as the ratio  $H_r = h_{fp} / h_{mc}$  (where  $h_{fp}$  and  $h_{mc}$  are the water depth in the floodplain and main channel, respectively). The water discharge was set upstream thanks to a gate valve. A honey comb was used to filter the fluctuations in the infilling tank and constrain the flow. A 1m long ramp was set at the upstream part of the flood plain; the equilibrium between the main channel and flood plain flows was expected to be obtained after 5m approximately (see section 2.3). The spur dyke was positioned at  $x=8.5\text{m}$  in order to modify a flow assumed in equilibrium. The downstream boundary condition (water depth) was fixed thanks to a tail gate. The description of the compound channel characteristics is presented in Figure 1 together with a schematic view of the flow around the spur dyke for a typical case with an impermeable spur dyke.

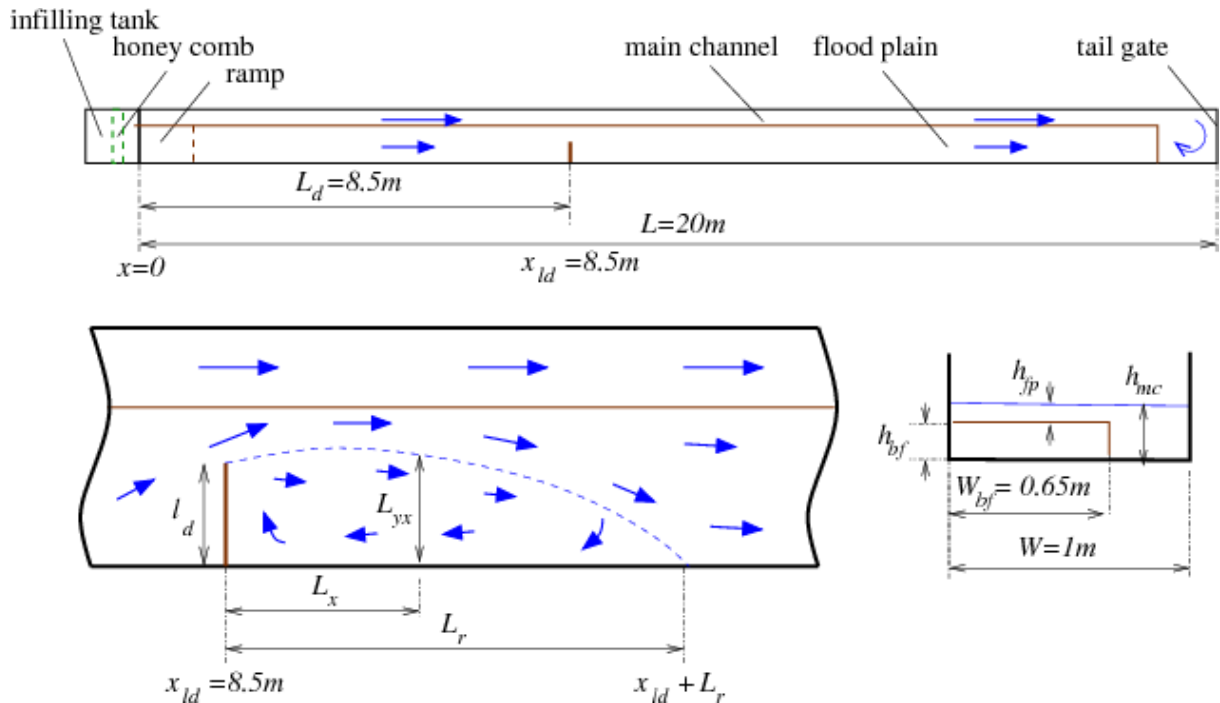
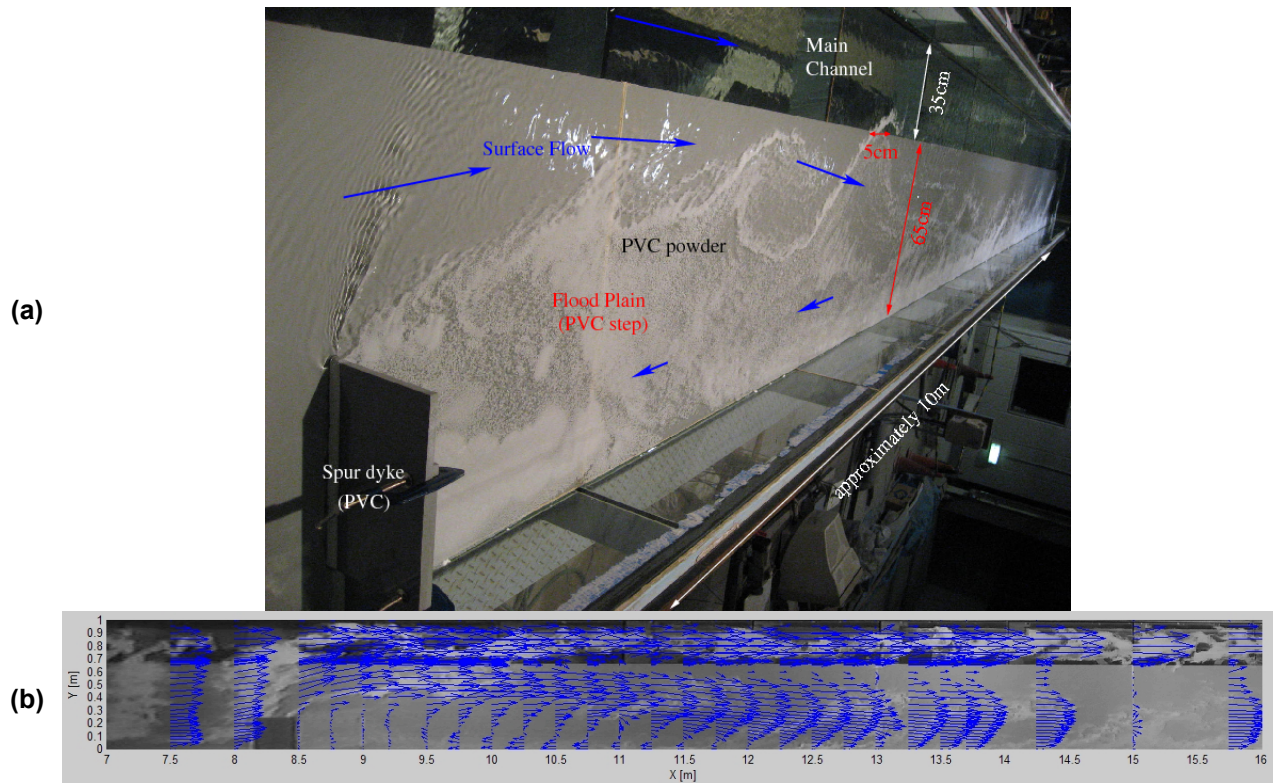


Figure 1: Compound channel characteristics and schematic view of the flow around the spur dyke (impermeable case).

### 2.2 Velocity measurements using LSPIV technique

Velocity measurements were carried out using the Large Scale Particle Image Velocimetry technique (Hauet et al., 2007) and an electromagnetic current meter (ECM). The LSPIV technique used in this study consists of four steps: First, a sequence of time-stamped digital images of the flow free-surface are evenly sampled with a fixed time interval between images. The camera was set on the structure of the laboratory, approximately four meters above the downstream part of the canal for the overall view of the canal. For detailed observations of the recirculation behind the spur dyke, the camera was set on a tripod on the side of the canal. Second, all the images are orthorectified, which consists of correcting perspective and lens distortion effects and of giving metric positions to transformed pixels. Third, the displacement of visible patterns in two successive orthorectified images is quantified using a simple cross-correlation algorithm (Fujita et al., 1998). Such visible patterns are assumed to be ideal

tracers of the surface flow velocity with minimal deformation between the two sampled images. For our specific case, artificial tracers (PVC powder, see Figure 2a) was injected to seed the flow. The displacements divided by the time step between images yield the surface velocities. The algorithms used for image orthorectification and cross-correlation velocity computation were developed by A. Hauet et al. (2007). Depth-averaged velocities at each node of canal was computed through i) interpolation or extrapolation of the surrounding LSPIV surface velocities and ii) multiplication by a float coefficient accounting for the vertical velocity distribution (Le Coz et al. 2010).



**Figure 2: Photo of the experimental set-up (a) and example of LSPIV results on a orthorectified image of the canal (b).**

The LSPIV allows the determination of the flow field in the channel assuming a relationship between the surface velocity and the mean velocity. The calibration of the LSPIV (float coefficient) was performed using measurements of the flow carried out with a electromagnetic current meter on four cross-sections along the canal: at  $x=x_{sd}=8.5\text{m}$  (section where the spur dyke was fixed),  $x=9.2\text{m}$  (section where the width of the recirculation reached its maximum), at  $x=x_{sd}+L_x+1$  (section where the flow in the flood plain is getting back to its equilibrium state) and at  $x=x_{sd}+(L_x+1)/2$  (section in the middle of the recirculation).

It appears clearly in Fig. 2a that the LSPIV method yields good results for the flow description around the spur dike as well as for the description of the recirculation. However, it is performing correctly only if there are enough tracers. Indeed, close to the main channel after the maximum width of the recirculation, the flow is divergent, and very few tracers cover this zone. As a result, the LSPIV method underestimates the surface velocities in this zone. As indicated in Table 1, the velocity in the main channel is from two to three times larger than the velocity in the flood plain. At the edge of the flood plain, there is a shear flow with the development of vortices. For a typical cross-section, the velocity should increase thus continuously from the middle of the flood plain to the middle of the main channel. Corrections of the results in this zone were undertaken using the results from the sections measured with the ECM.

### 2.3 Test cases carried out

The different cases studied in this paper are presented in Table 1. Two different length of the spur dyke were tested representing one third or one half of the flood plain. Larger length for the spur dyke would induce an interaction between the recirculation and the main flow that is too complex to study. Three different regimes were studied for  $H_r = 0.2, 0.3, \text{ or } 0.4$ . Totally, 13 experiments were undertaken, 3 cases in uniform flow (no spur dyke), 5 with an impermeable spur dyke and 5 with a permeable spur dyke (using the same conditions as the impermeable cases). The permeability of the permeable spur dykes was of 50%. For the specific water depth and mean velocities measured from the ECM, this table presents the results at the middle of the flood plain and of the main channel, respectively, for a section measured in the middle of the recirculation approximately, i.e. at  $x = x_{sd} + (L_x + 1)/2$ . For the uniform flow, the chosen section is the one at  $x=12.5\text{m}$ . For a permeable spur dyke, as no recirculation was observed, the same sections as the similar impermeable case were chosen for the measurements in order to be able to compare the results.

**Table 1: Description of the experiments carried out ( $h_{fp}$ ,  $h_{mc}$ ,  $V_{fp}$ , and  $V_{mc}$  are the mean water depths and velocities measured in the middle of the flood plain, and main channel, respectively at a x-position corresponding to the middle of the recirculation approximately).**

Test	$l_d$ [m]	$l_d / W_{fp}$ [-]	$H_r$ [-]	Q [l/s]	$h_{fp}$ [cm]	$h_{mc}$ [cm]	$V_{fp}$ [cm/s]	$V_{mc}$ [cm/s]	$L_r$ [m]
Uni02	-	-	0.2	9.51	1.32	6.36	10.8	42.4	-
Uni03	-	-	0.3	13.25	2.25	7.30	22.2	46.2	-
Uni04	-	-	0.4	20.85	3.57	8.64	33.3	48.9	-
Hr02d24i	0.24	0.37	0.2	9.51	1.04	6.07	3.1	44.2	2.10
Hr02d32i	0.32	0.49	0.2	9.51	0.90	6.06	0.3	44.8	2.40
Hr03d24i	0.24	0.37	0.3	13.25	1.90	7.01	18.4	49.5	4.25
Hr03d32i	0.32	0.49	0.3	13.25	1.62	6.85	9.3	52.4	5.00
Hr04d24i	0.24	0.37	0.4	20.85	2.79	7.87	30.9	62.6	5.20
Hr02d24p	0.24	0.37	0.2	9.51	1.15	6.26	8.7	40.9	-
Hr02d32p	0.32	0.49	0.2	9.51	1.13	6.20	7.6	42.4	-
Hr03d24p	0.24	0.37	0.3	13.25	2.08	7.22	22.4	43.7	-
Hr03d32p	0.32	0.49	0.3	13.25	2.07	7.17	17.4	47.7	-
Hr04d24p	0.24	0.37	0.4	20.85	3.30	8.47	33.4	49.8	-

## 3 RESULTS FROM THE LSPIV

### 3.1 An estimation of the bed evolution

Using the velocity fields obtained from the LSPIV measurements, an estimation of the potential sediment transport is possible. Assuming bedload transport proportional to the velocity  $V$  to the power 3 (that corresponds to the bed shear stress to the power 1.5 which is commonly used for the bedload formulas, Camenen & Larson, 2005) with a critical velocity for the inception of transport  $V_{cr}$ , local dimensionless sediment transport may be written as follows:

$$\bar{q}_s = \alpha(V^2 - V_{cr}^2)^{3/2} \frac{\bar{V}}{V} \quad (1)$$

where  $V$  is the velocity magnitude ( $V = \sqrt{V_x^2 + V_y^2}$ ), and  $\alpha$  a coefficient.

An estimation of the scour and sedimentation locations was suggested using the mass conservation equation:

$$\frac{\partial z}{\partial t} = \frac{1}{1-p} \left[ \frac{\partial q_s}{\partial x} + \frac{\partial q_s}{\partial y} \right] \quad (2)$$

where  $p=0.4$  is the porosity of the fictional mobile bed. For our specific case, a simple finite difference scheme was used to obtain an estimation of the bed evolution. As these study remains qualitative, a dimensionless bed evolution  $z/W$  will be used hereafter.

Of course, a movable bed made of sediment would influence the flow itself because of a larger roughness height. Considering the impact of a rough bed on the flow homogeneous, it can be assumed that velocity fields obtained from these experiments can give a good approximation of the velocity gradient, and so on the bed evolution. This method allows a macroscale observation based on mean velocities and does not include local effects such as those due to horse-shoe vortex in front of the structure or wake vortex behind permeable spur dyke (Zhang et al, 2009).

### 3.2 Results for an impermeable spur dyke

#### 3.2.1 Recirculation length

For the impermeable spur dyke, first results confirm the relationship between the ratio  $L_r / l_d$  and the friction number :

$$S = \frac{fl_d}{8h} \quad (3)$$

where  $L_r$  is the length of the recirculation behind the spur dyke,  $l_d$  the length of the spur dyke, and  $f$  the Darcy friction number with the exception of cases with small  $H_r$  and large  $l_d$  where the recirculation was interacting with the main channel flow. Depending on the  $S$  values, two asymptotic regimes are distinguished (Rivière et al., 2004; Peltier et al., 2008). When  $S < 0.01$ , the regime is called "Deep Water Flow" (DWF), the flow is controlled by the groyne and the length of the recirculation zone  $L_r$  is merely proportional to  $l_d$  with  $L_r \approx 20 l_d$ . When  $S > 0.1$ , the regime is called "Shallow Water Flow" (SWF), the physics is controlled by bed frictions ( $L_r \approx 5 h/f$ ). A general equation for the recirculation length writes:

$$\frac{L_r}{l_d} \approx \begin{cases} 20 & \text{if } S < 0.01 \\ 0.6 S^{-1} & \text{if } S > 0.1 \end{cases} \quad (4)$$

Figure 3 presents for different experiments the length of the recirculation behind the spur dyke made dimensionless with the length of the spur dyke  $L_r / l_d$  as a function of the friction number  $S$ . The Darcy-Weisbach friction coefficient was estimated using hydraulic parameters measured in the flood plain for the equivalent uniform flow ( $f/8 = g h_{fp} S_0 / U_{fp}^2$  where  $g$  is the acceleration of the gravity and  $S_0$  the slope of the flood plain). It appears that the new data set is well described by the theory (Equation 4) and is in good agreement with previous data from Peltier et al. (2008, data from LMFA and CNR). Most of the present data appear to be in the SWF regime or in an intermediate regime. As observed by Rivière et al. (2008) for channel expansions, the recirculation length in the DWF regime appears to be a function of the Froude number and of the ratio  $W/l_d$  where  $W$  is the width of the flume. For the case of a compound channel, similar behaviour may be observed. The plateau for  $L_r / l_d$  seems to be not as high for some other experiments especially for  $H_r=0.4$ .

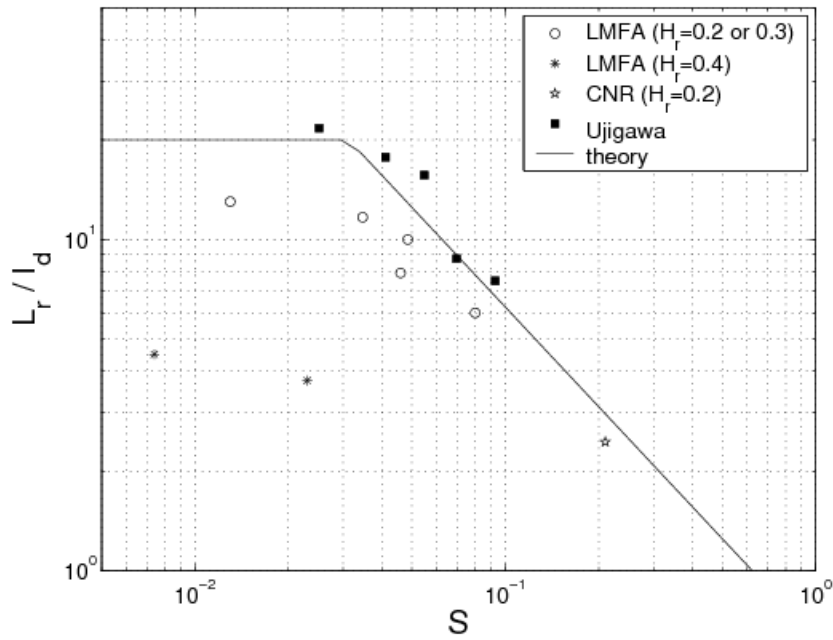


Figure 3: Length of the recirculation behind the spur dyke made dimensionless with the length of the spur dyke  $L_r/l_d$  as a function of the friction number  $S$ .

### 3.2.2 Main characteristics of the bed evolutions, effect of the critical velocity for the inception of transport

Figure 4a presents the results obtained for the velocity field for the test case with  $l_d = 0.24\text{m}$  and  $H_r = 0.2$  including the corrections of the divergent flow (see section 2.2). The recirculation zone is easily observable with a maximum width at the position  $x = 9.2\text{ m}$ . For this specific case, the velocities in the recirculation zone are very weak. A similar position of this maximum width was observed for all the cases indicating the strong influence of the main channel flow on this value. For a larger length of the spur dyke ( $l_d = 0.40$  was also tested), the width of the recirculation zone reached the main channel. A much more complex dynamic of the recirculation was then observed. For  $x > x_{ld} + L_r$ , the flow become divergent until the end of the recirculation zone ( $x > x_{ld} + L_r$ ). The uniform flow (in term of mean velocities) is reached only after 5 or 6 meters after the end of the recirculation zone.

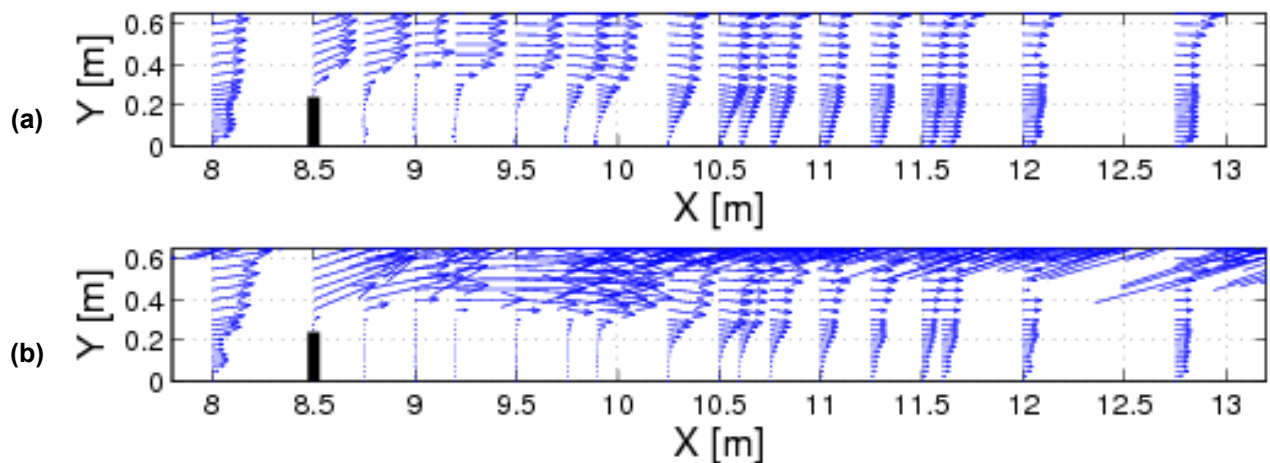
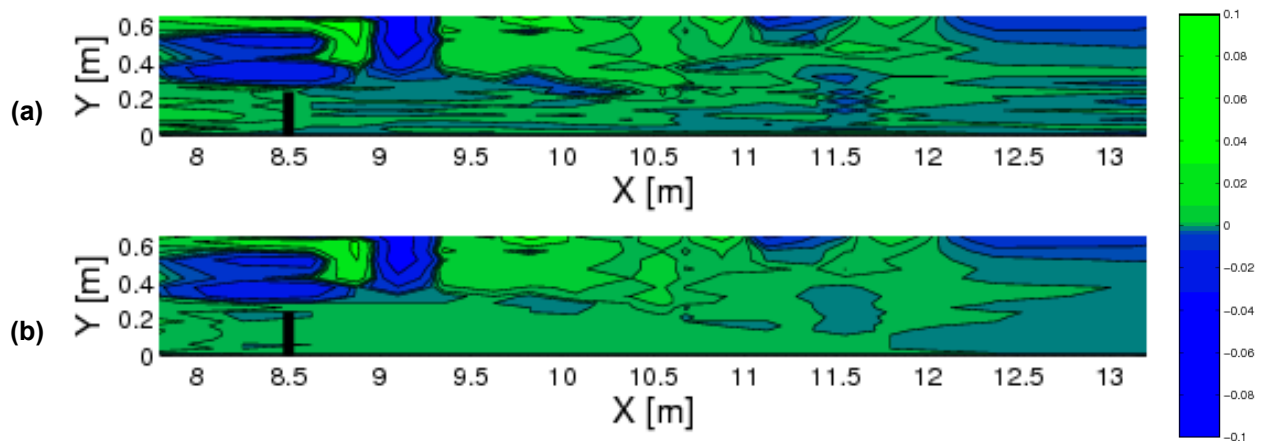


Figure 4: Corrected velocity from LSPIV measurements (a), dimensionless bedload transport (b) for the test case with  $l_d = 0.24\text{m}$  and  $H_r = 0.2$ .

From the velocity field, the estimation of a dimensionless bedload transport can easily be obtained using Equation 1. Assuming first that  $V_{cr}=0$ , it appears that the effect of the recirculation zone on the bedload transport field is emphasized compared to the velocity field (see Figure 4b). From the velocity distributions in Figure 4b, very large spatially variations of the bedload transport in the flood plain are expected with nearly no transport in the recirculation zone. And the maximum bedload estimated in the flood plain is generally much lower than the typical values observed in the main channel. For this reason, the study will be more focused on the flood plain.

In Figure 5a, the dimensionless bed evolution derived using Equation 2 is plotted for the test case with  $l_d = 0.24\text{m}$  and  $H_r = 0.2$  using a critical velocity  $V_{cr} = 0$ . Significant erosions are estimated in two areas due to the flow acceleration; one is at the foot of the spur dyke and the other above the recirculation with its maximum width ( $x=9.2\text{m}$ ). On the other hand, large deposition may be observed between two areas above and the downstream to the maximum width of the recirculation. Some deposition is also observed upstream of the spur dyke because of the decrease of the flow magnitude. Because of the very low dynamics within the recirculation zone, nearly no variation of the bed is expected. However, if we consider suspended load and no bedload transport, this zone would be typically a deposition zone for very fine sediments. The shear flow induced by the interaction between the main channel and the floodplain yields also a much more active bed dynamics at this location, which is very sensitive to the modification of the flow induced by the spur dyke. The small erosion observed at the section  $x = 11.5\text{ m}$  seems to be a spurious effect of the LSPIV velocity correction or because of the imperfections of the joints between two PVC plates forming the flood plain (at the section  $x = 11.0\text{ m}$ ).

In Figure 5b, the dimensionless bed evolution is plotted for the test case with  $l_d = 0.24\text{m}$  and  $H_r = 0.2$  using a critical velocity  $V_{cr} = 0.1$ . This critical value affects mainly the recirculation zone where very low dynamics were observed. Because of this critical value, the zone is now motionless. A value  $V_{cr} = 0$  will be fixed hereafter.



**Figure 5: Dimensionless bed evolution for the test case with  $l_d = 0.24\text{m}$  and  $H_r = 0.2$  using a critical velocity  $V_{cr} = 0$  (a) or  $V_{cr} = 0.1$  (b).**

### 3.2.3 Effect of the size of the spur dyke

In Figure 6a, the dimensionless bed evolution was plotted for the case with a longer spur dyke ( $l_d = 0.32\text{m}$ ). The length of the spur dyke does not affect significantly the deposition/erosion distribution and amplitude. Compared to the case with a shorter spur dyke (see Figure 5a), Very similar results are obtained. Only the width of the main erosion and deposition zones is lower as the distance between the spur dyke foot and the main channel is shorter. As observed before, the length of the spur dyke has also a minor effect on the length of the recirculation (see table 1).

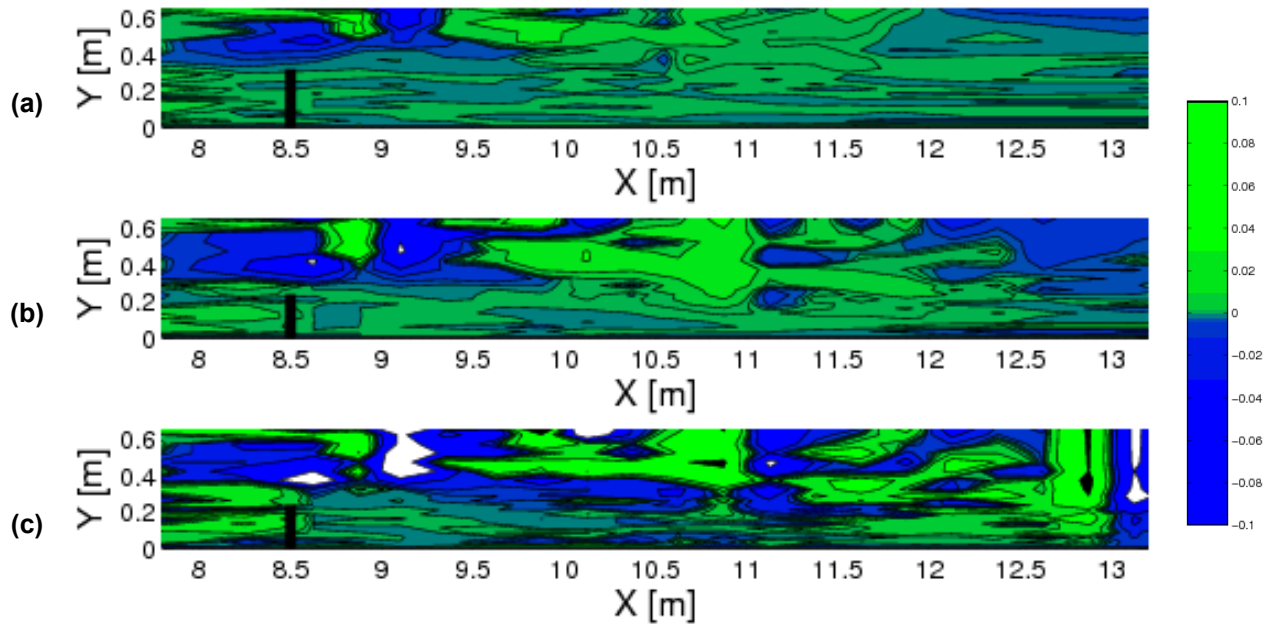


Figure 6: Dimensionless bed evolution for the test case with  $l_d = 0.32m$  and  $H_r = 0.2$  (a) with  $l_d = 0.24m$  and  $H_r = 0.3$  (b) with  $l_d = 0.24m$  and  $H_r = 0.4$  (c) ( $V_{cr} = 0$ ).

### 3.2.4 Effect of the discharge or water depth ratio $H_r$

In Figure 6b and c, the dimensionless bed evolution was plotted for cases with water depth ratios ( $H_r = 0.3$  and  $H_r = 0.4$ , respectively). In the same way as for the length of the spur dyke, the water depth ratio does not affect significantly the deposition/erosion distribution. As the length of the recirculation seems to be sensitive to  $H_r$  (see table 1), the deposition zone in the convergent flow is getting larger with the ratio  $H_r$ . Also, velocities in the flood plain are getting larger for  $H_r = 0.3$  and  $H_r = 0.4$  especially. Bedload transport and induced bed evolution have thus much larger magnitude (zones in white and black correspond to values smaller than  $-0.1$  and higher than  $0.1$ , respectively).

For the case with  $H_r = 0.4$ , the erosion zone develops all around the recirculation zone. Moreover, as the flow in the recirculation is getting higher (development of a return flow close to the wall, see Figure 7), bedload transport is not negligible anymore and some erosion/deposition zones appears within the recirculation zone.

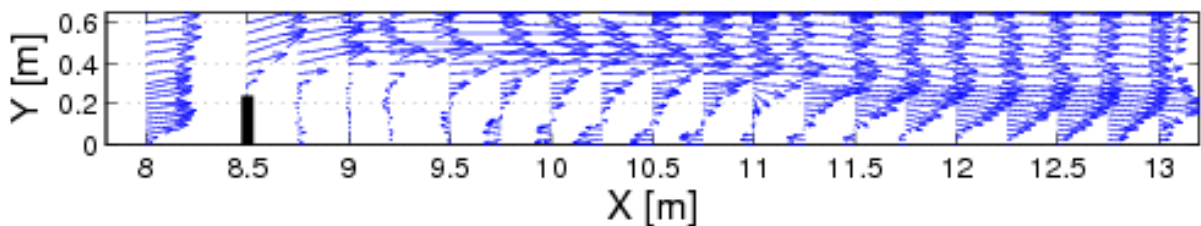


Figure 7: Corrected velocity from LSPIV measurements for the test case with  $l_d = 0.24m$  and  $H_r = 0.4$ .

### 3.3 Results for an permeable spur dyke

In case of the permeable spur dyke, effects are roughly similar to those of the impermeable spur dyke but weaker. A weak erosion may be observed at the foot of the spur dyke. However, it is partly due to a spurious effects due to the vortices developing from the foot of the spur dyke. ECM measurements showed a continuously increasing velocity from the right bank to the left bank at this position. The deposition zone upstream to the obstacle is also wider than for the case with an impermeable spur

dyke. Downstream to the obstacle, there is no recirculation but a slowly increasing flow is observed, inducing some small erosion. In the same way as for the previous cases, the imperfections of the joints between two PVC plates forming the flood plain at the section  $x = 11.0$  m seems to affect the results of the LSPIV, inducing spurious effects in the velocity fields and so in the bed evolution.

As a consequence the permeable spur dyke appears to be a more interesting alternative as the impermeable spur dyke in term of morphodynamics.

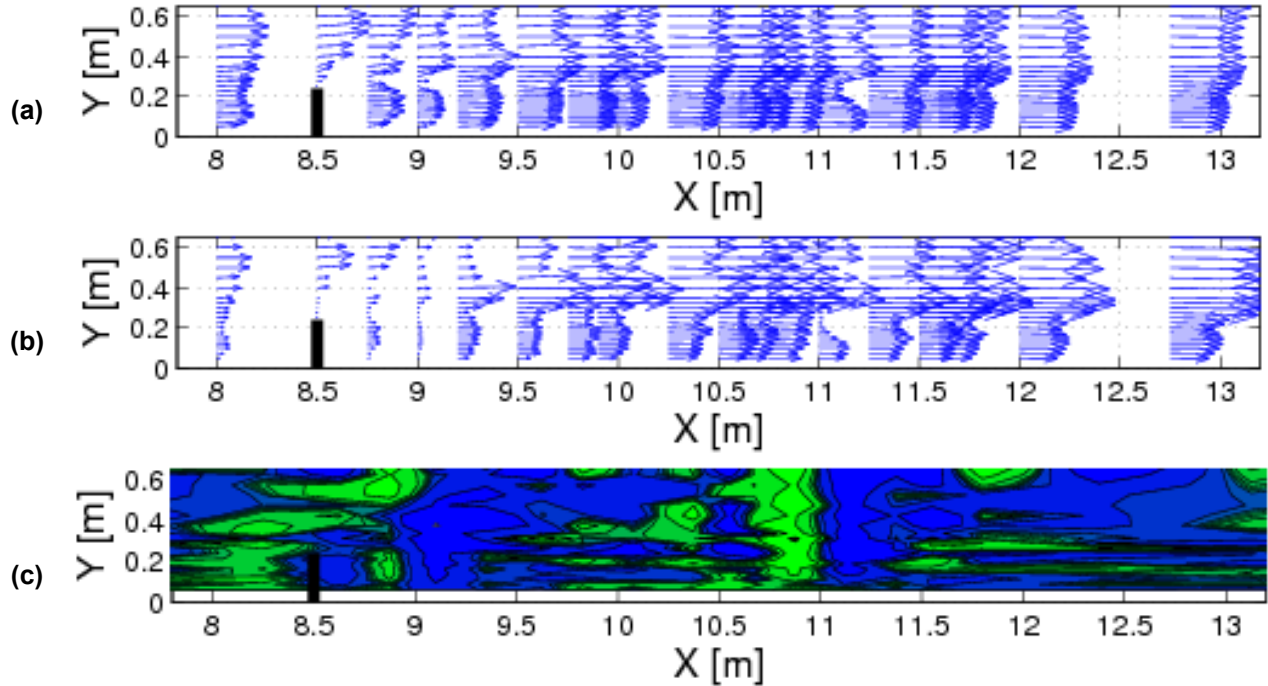


**Figure 4: Corrected velocity from LSPIV measurements (a), dimensionless bedload transport (b), and dimensionless bed evolution (c) using a permeable spur dyke for the test case with  $I_d = 0.32$  m and  $H_r = 0.2$ .**

#### 4 DISCUSSION

The main effects of an impermeable spur dyke on the flow are the following:

- relative weak magnitude of the velocity in the upstream part of the spur dyke
- large velocities around the obstacle with a strong shear flow at the foot of the spur dyke
- nearly no velocities in the recirculation zone

The weak velocities in the recirculation area downstream of the spur dyke as well as in the upstream part of the spur dyke yield a considerable potential of deposition in both areas.

On the other hand, the strong magnitude of the velocity is observed around the foot of the spur dyke due to the convergence of the flow in each experimental condition. The shear flow induced by the interaction between main flow and recirculation area would yields a much more active bed dynamics at this location. These flow characteristics illustrate the potential bottom profile change, which would lead to generate local scour and deposition. Figures 5 and 6 displays the contours of the estimated bed evolution derived by Equations 1 and 2. It is obvious from these figures that erosion and deposition areas would be generated around the spur dyke and the recirculation area.

In the experimental result around a non-submerged spur dyke with movable bed condition (for example, Zhang et al, 2009), locally bed deformation (local scour around the spur dyke and the deposition downstream of it) is clearly observed around the spur dyke. These typical bed evolutions (local scour and deposition) are produced as a result of the interaction between flow characteristics and bed evolution. There are however adding 3D effects (horse-shoe vortex upstream the obstacle and wake vortex downstream the obstacle), which induce erosion close to the obstacle. These erosion are not observed by the LSPIV measurements. The experimental results in Figures 5 and 6 indicate the development of the scouring and deposition around the spur dyke although those don't provide full explanation for the bed evolutions under movable bed condition.

In case of the permeable spur dyke, the flow patterns around the spur dyke present quite different behaviour from the one with an impermeable spur dyke. The effects of the spur dyke on the flow are the following:

- relative weak magnitude of the velocity in the upstream and downstream parts of the spur dyke
- a weak shear flow around the foot of the spur dyke

No recirculation area is observed downstream of the spur dyke and the velocity downstream of the spur dyke increase gradually in the downstream of the spur dyke. These results are confirmed by other experimental results (for example, Zhang et al, 2008). In case of the permeable spur dyke, a local scour still exists around the spur dyke. However, the magnitude of the scouring and the eroded area is generally smaller than those in the impermeable case. This result indicates low probability of a severe erosion around the permeable spur dyke, and the permeable spur dyke appears to be a more interesting alternative as the impermeable spur dyke in term of morphodynamics.

## 5 CONCLUSION

This paper presented some experimental results around the non-submerged impermeable spur dyke and discusses the influence of the spur dyke on the flow characteristics and on the estimated bed evolutions based on the potential bedload transport.

The spur dyke was set on the floodplain of a compound channel, which was built in a 20m long straight experimental flume. Two types of spur dyke set on the floodplain were used in the experiments, one is impermeable and the other permeable (pile groin with a permeability of 50%). Totally, 13 experiments were undertaken with some different conditions of the length of the spur dyke, the ratio of the water depth in the floodplain and main channel  $H_r$  and the type of spur dyke.

The main results are as follows:

The relationship between the ratio  $L_r / l_d$  and the friction number given by Equation 3 is confirmed with the exception of cases with small  $H_r$  and large  $l_d$ , for which an interaction between the recirculation and the main channel was observed. It is found from the experimental results that the new data set presented here is well described by the previous theory (Equation 4) and is in good agreement with previous data from Peltier et al. (2008, data from LMFA and CNR). Most of the present data appear to be in the SWF regime or in an intermediate regime.

In case of the impermeable spur dyke, the velocity distributions in the recirculation area downstream of the spur dyke have relative weak magnitude as well as in the upstream part of the spur dyke. On the other hand, velocities of large magnitude were observed around the foot of the spur dyke due to the convergence of the flow in each experimental condition. Using the velocity distributions, the bed evolutions around the spur dyke are estimated with a simple relationship between the flow velocity and the potential sediment transport (Equations 1 and 2). The estimated bed evolutions indicate the development of the scouring and deposition around the spur dyke although the experimental results presented here don't provide full explanation for the bed evolutions under movable bed condition as they don't include 3D effects.

In case of the permeable spur dyke, the flow patterns around the spur dyke present completely different behaviour compared to the impermeable spur dyke. The results in the bed evolution are in

good agreement with other experimental results (for example, Zhang et al, 2008). A local scour still exists around the permeable spur dyke. However, the magnitude of the scouring and the eroded area is smaller than those in the impermeable case. This result indicates low probability of severe erosion around the permeable spur dyke, and the permeable spur dyke appears to be a more interesting alternative as the impermeable spur dyke in term of morphodynamics.

## 6 ACKNOWLEDGEMENT

The authors express their appreciation for the support of all members joining this joint research program. These experiments were partially supported by the bilateral program Sakura from the Japan Society for the Promotion of Science (JSPS) and Hubert Curien Partnership (PHC).

## 7 REFERENCES

- B. Camenen & M. Larson (2005). A bed-load transport formula for the nearshore, *Estuarine Coastal and Shelf Science*, vol. 63, pp. 249-260.
- I. Fujita, M. Muste, & A. Kruger (1998). Large-scale particle image velocimetry for flow analysis in hydraulic engineering applications. *Journal of Hydraulic Research* 36 (3), 397–414.
- A Hauet, JD Creutin, & P Belleudy (2007). Sensitivity analysis of large-scale particle image velocimetry measurement of river discharge using numerical simulation, *Journal of Hydrology*, 349(1-2), 178-190.
- Le Coz, J., Hauet, A., Dramais, & G., Pierrefeu, G., 2010. Performance of image-based velocimetry (LSPIV) applied to flash-flood discharge measurements in Mediterranean rivers, submitted to *Journal of Hydrology* (subm. 1 September 2009, revised Jan. 2010, Special Issue Flash-floods).
- Y Peltier, S Proust, A Bourdat, F Thollet, N Rivière, & A Paquier (2008). Physical and numerical modeling of overbank flows with a groyne on the floodplain. *Proc. of the International Conference on Fluvial Hydraulics, River Flow, Cesme-Izmir, Turkey, September 3-5, 2008*, Altinakar, Kokpinar, Aydin, Cokgor & Kirkgoz (eds), 1, 447-456.
- N. Rivière, B. Badin, Y. Bomchil, & S. Proust (2008). Recirculation zones downstream open channel expansions. *Proc. of the 4<sup>th</sup> Int. Conf. on Fluvial hydraulics, River flow 2008, Sept. 3-5, Cesme-Izmir, Turkey*, pp. 2233-2238.
- N. Rivière, S. Proust & A. Paquier (2004). Recirculating flow behind groynes for compound channel geometries. *Proc. of the 2<sup>nd</sup> Int. Conf. on Fluvial hydraulics, River flow 2004, June 23-25, Napoly, Italy, Greco, Carravetta & Della Morte (eds.)*, pp. 437-442.
- H. Zhang and H Nakagawa (2008). Investigation on morphological consequences of spur dyke with experimental and numerical methods, *Proc. 8<sup>th</sup> Int. Conf. on Hydrosience & Eng.*, pp.1490-1499.
- H. Zhang, H Nakagawa, K Kawaike, & Y Baba (2009). Experiment and simulation of turbulent flow in local scour around a spur dyke. *Int. J. Sediment Res.*, 24(1) 33-45.